Thermal imaging of Volcanic Areas and implications for the Interpretation of surface temperatures on Mars.
K. Kurita[1], D. Baratoux[2], H. Sato[1,2], A. Suzuki[2], J. Vaucher[1,2], S. Kodama[3], M. Ichihara[1], K.Saiki[4] , T. Kaneko[5] , J. Kimura[1], S.Takahashi[1], R. Nakamura[6], H. Watanabe[5]; [1]Earthquake Research Institute, University of Tokyo, 113-0032, 1-1-1, Yayoi, Bunkyo-ku, Tokyo, Japan (kurikuri@eri.u-tokyo.ac.jp), [2]Observatory Midi-Pyrénées, Laboratory Dynamique Terrestre et Planétaire, UMR 5562, CNRS and University Paul Sabatier Toulouse III, 31 400 Toulouse, France (baratoux@dtp.obs-mip.fr). [3]Geology Information Center, . [4]Department of Earth and Space Science, Osaka University, 1-1 Machikaneyama-cho,Toyonaka-shi,Osaka 560-0043,Japan, [5]Volcano Research Center at Earthquake Research Institute, University of Tokyo, 113-0032, 1-1-1, Yayoi, Bunkyo-ku, Tokyo, Japan.

Introduction: The observation of the Mars surface with the THEMIS instrument onboard of the Mars Odyssey has demonstrated the value of thermal observations for the understanding of planetary surface processes [1]. However, two important issues remain concerning these observations. (1) Despite numerous theoretical and experimental efforts to understand the physics of thermal conductivity of granular material, it is still difficult to interpret thermal inertia observations. The thermal inertia values are often simply related to mean particle diameter through laboratory measurements of monodisperse particles under the Martian atmospheric conditions, even if mixtures of different particles sizes have been studied recently [2]. (2) One of the objectives of the THEMIS experiment was also to detect subsurface heat sources associated with recent volcanic or hydrothermal activity on Mars. However, all the THEMIS observations have been so far interpreted in terms of thermal inertia variations. Even on the earth, which is known to be volcanically active, it's not certain that the full coverage of the planet with thermal measurements integrated at the 100 meters scale will evidence any activity, with a possible exception for the mid-oceanic ridges. We thus started a project named TIMVAS (*for Thermal Imaging of Volcanic Areas*) using joint and simultaneous observations with thermal probes at different depths and thermal cameras. The thermal observations were done in Japan at Oshima and Kusatsu volcanoes during August and September 2006.

This project has two objectives. (1) A first aspect is to improve our understanding of the factors controlling the thermal conductivity of porous material focusing on the volcanic products which are widespread on Mars. The volcanic sites were selected for their diversity on fresh volcanic products (including porous volcanic rocks, scoriae, ashes, and volcanic sands). The second part aims to be able to separate the contribution of the energy balance at the surface from the contribution of subsurface heat source from the thermal modeling of the observations. Subsurface heat sources can be potentially observed at the surface through heat conduction, but this contribution is expected to be low relatively to the flux resulting from heating by the sun light. However, larger contributions are expected from potential circulations of fluids in the porous media, an idea which is developed in a companion paper [3]. The results are currently applied to Mars with the objective to find subsurface heat flow anomalies in areas where recent or event present volcanism is suspected.

A brief review of the thermal conductivities of granular material: A considerable amount of work has been done toward the understanding of the thermal conductivity of granular material. Granular material is usually considered as a two phase material composed by a solid and a gas component. The conductivity of the solid phase, usually well known, is noted here k_s. The conductivity k_p corresponds to the effective conductivity of pores filled by a fluid phase. It depends on the conductivity of the gas inside the pores, but also on the radiative exchange within the pore surfaces. Thus, $k_p = k_f + k_r$, where k_f is the conductivity of the fluid phase and k_r is the radiative term. The radiative term is a function of the temperature of the solid. The fluid term is a function of pressure and temperature. Let's now consider the conductivity of two phase material, k_s and k_p. The volume fraction associated with k_p in the material is noted ϕ (porosity). Various models can be found in the literature, and the review given here demonstrates the needs for further work toward the understanding of the thermal conductivity of granular media.

- *Porosity with pores in series.* The pores are represented by layers perpendicular to the direction of the heat flow. The thermal conductivity is given by:

$$k = \frac{1}{\frac{\phi}{k_p} + \frac{1-\phi}{k_s}}$$

- *Porosity with pores in parallel*. The pores are represented by layers parallel to the heat flow. The thermal conductivity is given by:

$$k = k_p\phi + (1-\phi)k_s$$

- *The Loeb's model* [4] considers pores parallel and perpendicular to the direction of the heat flow. Thus, the conductivity is a function of two porosities ϕ_1 and ϕ_2:

$$k = k_s - k_s\phi_1 \frac{1 - \frac{4\gamma\epsilon\sigma d\bar{T}^3}{k}}{1 + \frac{4\gamma\epsilon\sigma dT^3}{k}\frac{1-\phi_2}{\phi_2}}$$

- *The Russel's model* [5] considers the porous material as cubes in a different medium.

$$k = k_s \frac{\phi^{\frac{2}{3}} + \frac{k_s}{k_p}(1-\phi^{\frac{2}{3}})}{\phi^{\frac{2}{3}} - \phi + \frac{k_s}{k_p}(1-\phi^{\frac{2}{3}}+\phi)}$$

- *The Beck's model* [6] is an adaptation of the Maxwell's model to the thermal conductivity of biphasic material:

$$k = k_s \frac{(2\frac{k_s}{k_p}+1)-2\phi(\frac{k_s}{k_p}-1)}{(2\frac{k_s}{k_p}+1)+\phi(\frac{k_s}{k_p}-1)}$$

- *Geometric mean model*. The geometric model can be considered as an approximation of the Beck's formula, even is it does not have a physical basis:

$$k = k_p^{\phi} k_s^{1-\phi}$$

- *Porosity model*. The conductivity was fitted using few thermal measurements on sandstone:

$$k = k_s(1-\phi^4)$$

- *An empirical model based on the arithmetic mean* has been proposed by [7] :

$$k = (1-A)k_s + Ak_p$$
$$A = [2^n(2^n-1)^{-1}][1-(1+\phi)^{-n}]$$

- *The Brailford and Major's model* [8], which was derived later but independently by Sirono and Yamamoto considers a distribution of sphere with a continuous medium [9]. The conductivity is given by:

$$k = \frac{[(3\phi-1)k_1 + (2-3\phi)k_2] + \sqrt{[(3\phi-1)k_1 + (2-3\phi)k_2]^2 + 8k_p k_s}}{4}$$

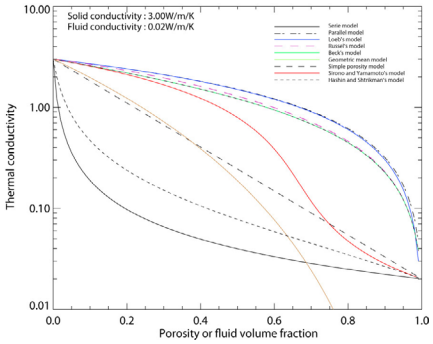

Fig. 1. Comparisons of different models of thermal conductivity for granular material (terrestrial conditions, k_{air} = 0.02 W/m/K, k_{rock} = 3 W/m/K).

Another approach has been followed in preparation of the Mars data analysis. Under a wide range of pressure (0.001 to ~133 bars), it has been shown that the thermal conductivity depends on the mean grain size of particles [10]. However, the preparation of the samples mentioned in [10] shows that grain size changes are also related to porosity changes. The considerable differences (cf. Fig.1) in physical models strongly justify the achievements of new thermal measurements of granular soils, both in the field and in laboratory.

Thermal observations of volcanic landforms on the Earth: Thermal conductivity measurements on natural samples can be done in controlled environment in the laboratory or in the field. Since our objective is to separate the different contributions controlling the surface temperature, we have achieved a survey of surface and subsurface temperature evolution over one or more diurnal cycles from simultaneously thermal probes and thermal cameras. We first report on the derivation of the thermal inertia and conductivity of the volcanic soils.

First approach: direct modelling of subsurface temperature. The temperature measurements at two different depths are used to derive the effective thermal conductivity within these two points. One measurement at a given depth is used as a boundary condition. A direct modelling is achieved to estimate the temperature at the depth of the second sensor with different values of thermal conductivities.

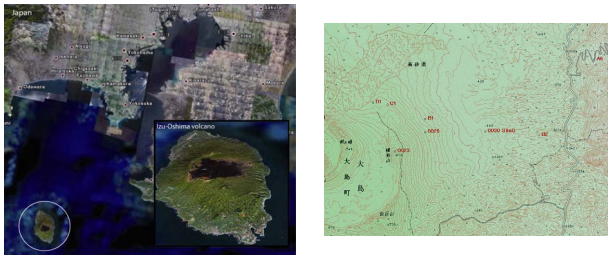

Fig. 2. Left: Izu-Ohsima Island in Japan selected for its diversity of volcanic products and grain sizes mostly free of vegetation. Recent eruptions suggest the possible contribution of subsurface heat sources. Right: Topographic map of the eastern flank of the Oshima volcano with the localization of the sites where temperature measurements have been achieved.

The thermal diffusivity is derived from the minimization of differences between the model and the observations. We write:

$$z' = \frac{z}{\sqrt{\kappa P}} \qquad t' = \frac{t}{P}$$

where *P* is the duration of the diurnal cycle (86400 *s*). With these non-dimensional variables the conduction equation writes:

$$\frac{\partial T}{\partial t'} = \frac{\partial^2 T}{\partial z'^2}$$

Then, for each couple of sensors at two different depths (Fig. 3), differences between model and observed temperatures are estimated as a function of the thermal diffusivity and time (Fig. 4). The time-averaged differences versus thermal diffusivity are represented in Fig. 5, the minimum of this function corresponding to our estimation of the thermal diffusivity. In this case, the subsurface temperature evolu-

tion is explained by a thermal conductive model with a constant conductivity. The optimal thermal diffusivity is about 7.10^{-7} m/s^{-2}. Changes in thermal diffusivities are reported at other sites and also when different depths are used. This suggests possible significant variation of the thermal properties within the first 30 centimes of the soil. Some observations presented later the subsurface temperature are not explained by the thermal conduction alone.

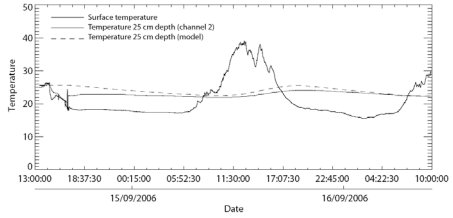

Fig. 3. Temperature at 25 cm from surface temperature at site B1. The model corresponds to the best fit at 25 cm depth with a thermal diffusivity =7.10^{-7}).

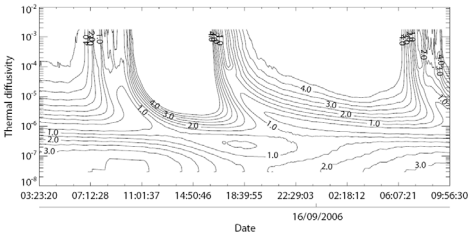

Fig. 4. Differences of the observed temperatures at 25 cm depth and the model temperatures as a function of the thermal diffusivity and time.

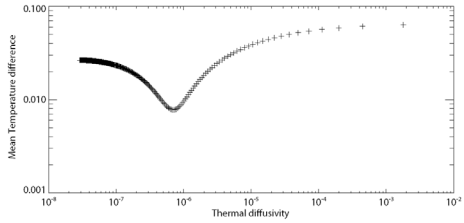

Fig. 5. Time-averaged differences (model/ observation at 25 cm depth) versus thermal diffusivity.

A simple model for the temperature evolution at the sun set. Alternatively, it is possible to evaluate the thermal inertia from the following assumptions. Few hours after the sunset, it is observed that the surface heat flow is constant. Consider the energy balance for a slab of material (cf. Fig. 3) having a temperature T_0 at the time t=0. Consider the slab at the time t. The temperature at the surface is T_s(t).

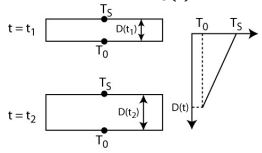

Fig. 6. A simple model for the temperature evolution at the sunset.

The thickness of the slab is defined such as the temperature at the bottom of the slab is equal to T_0 (progression of the cooling front) and the measured surface temperature is T_s. The heat lost in the slab is given by:

$$H = \frac{1}{2}\rho C D(t)(T_0 - T_s(t))$$

where C and ρ are the specific heat and mass density of the slab material, D(t) is the depth of the cooling font. This heat corresponds to the integration of heat flux at the surface between 0 and t, the temperature gradient being constant. Considering that the heat flux at the surface is constant few hours after the sunset:

$$H = k\frac{T_0 - T_s(t)}{D(t)}t$$

where k is the thermal conductivity. Eliminating $D(t)$ in both equations, we find:

$$T_s = T_0 + \frac{\sqrt{2}}{\sqrt{k\rho C}}Gt^{\frac{1}{2}} = T_0 + \frac{\sqrt{2}}{I}Gt^{\frac{1}{2}}$$

where G is the heat flux and I is the thermal inertia of the material. Thermal inertia estimation requires the knowledge of G. For an estimated value of 30 W/m^2, the thermal inertia at B1 is 1760 Js$^{-1/2}$K^{-1}m^{-2}, and 660 Js$^{-1/2}$K^{-1}m^{-2} at B2.

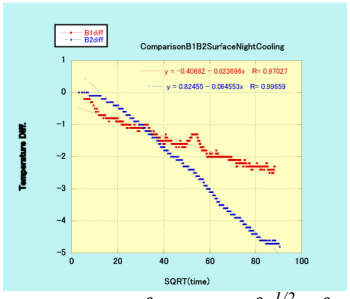

Fig. 7. Temperature as function of $t^{1/2}$ after the sunset for two experiments. Note the linear evolution of the temperature with $t^{1/2}$. The thermal inertia at B1 is higher than the thermal inertia at B2.

Derivation of thermal diffusivity from Fourier analysis. A third approach consists in the derivation of thermal diffusivity from the Fourier analysis of temperatures at different depth. The signal is decomposed following:

$$T(z,t) = T_0 + \sum_{n=1}^{\infty} A_n e^{i\omega t + \phi_n - i\sqrt{\frac{\omega n}{2\kappa}}z} e^{-\sqrt{\frac{\omega n}{2\kappa}}z}$$

where T_0 is the mean temperature, ω is the pulsation, z is the depth, and A_n is the amplitude of the surface temperature for the component n. The phase shift and the amplitude ratio of the different component depends on the thermal diffusivity κ. The main limitation of this approach is the fact that the surface temperature is not exactly a periodic function of time over the duration of the experiment (side effect are expected). Amplitude ratios are given in the Fig. 8. Syntheses of the different approaches are presented in the Table 1.

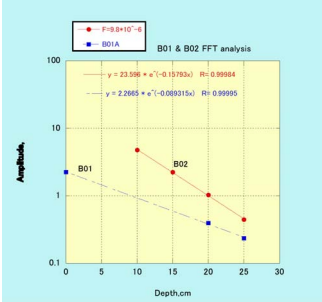

Fig. 8. Amplitude ratio as a function of depth to retrieve the thermal diffusivity (n = 1).

Site	Material type	κ (direct)	T.I	κ (FFT)
B1	Coarse grained scoria	$4.7*10^{-7}$ $6.9*10^{-7}$	1760	$4.1*10^{-7}$
B2	Fine grained scoria	$< 10^{-7}$?	655	$1.2*10^{-7}$

Table 1: Synthesis of thermal inertia/diffusivity estimations. Consistent values are found for B1 (assuming ρ = 2700 kg/m^3 and C_p = 840 J/kg/K). As presented later, the site B2 is difficult to interpret in terms of conductive processes only.

Addition contributions. We report on few sites where the subsurface temperature evolution is not explained by the conduction process alone (see Fig. 9, temperature at z = 0 and z = 20 cm Fig. 9). Optimal thermal conductivities would be different between day and night to explain both the increase of surface temperature during the day and the constant temperature during the night. We are currently investigating the role of other contributions. The likely sources are subsurface gas flow [3] or H_20 phase transtion. The error in the estimation of the surface temperature requires an assessment, but it can not probably explain both day and night behaviors.

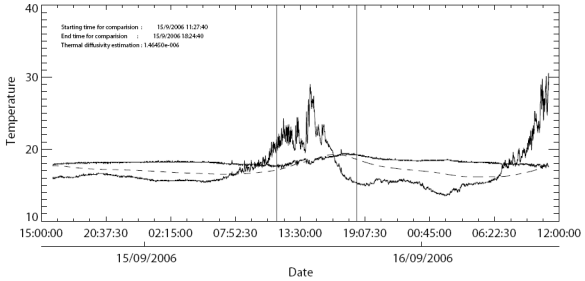

Fig. 9. Surface temperature and subsurface temperature at 20 cm depth from the site B2.

Thermal survey of Oshima. Thermal images have been acquired at the Caldera of the Oshima volcano in order to map the thermally active zones (fumerolles). We also report on the important control of the lithology on the surface temperature. The Fig. 10 and 11 represent the temperature at wall of the Oshima caldera at the sunset. The surface temperature variations clearly follow the alternance of layers of various volcanic deposits, grain size, or degree of compaction.

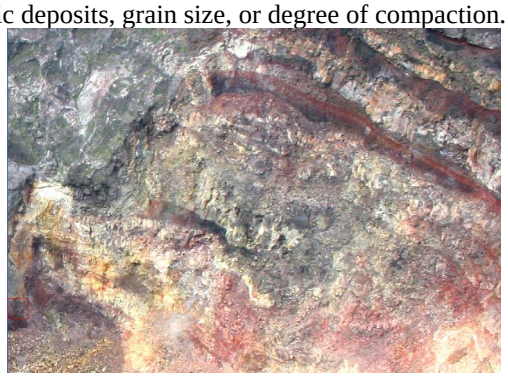

Fig. 10. Picture of the volcanic layers exposed at the wall of caldera of Oshima volcano (h = 20 meters).

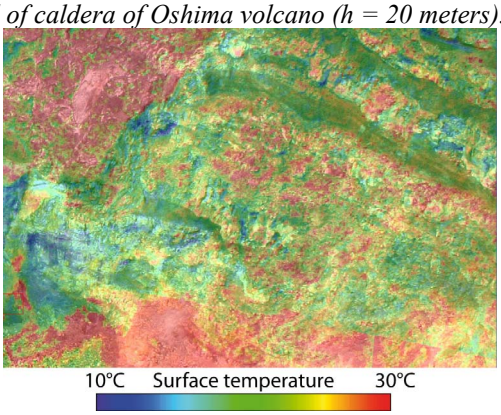

Fig. 11 Surface temperature at the sunset superimposed on the image of the caldera wall. This result shows the clear correlations between lithology and thermal properties for the volcanic material.

Conclusions. This report focused on the thermophysical properties of volcanic materials on the Earth, and the implications of the thermal imaging of volcanic landforms on Mars. It is hoped that further work will help us to discriminate between the various possible volcanic products (ash, lava flow, sands etc…) presents on Mars. A most challenging part and consequence of this project is the potential identification of subsurface heat source of Mars related to recently volcanically active areas.

References: [1] Fergason, R. L. et al. (2006), *J. Geophys. Res.*, 111, E12004, doi:10.1029/2006JE002735. [2] Presley, M. A., and R. A. Craddock (2006), *J. Geophys. Res.*, 111, E09013, doi:10.1029/2006JE002706. [3] Antoine et. al, this issue. [4] A.L. Loeb, *J. Am. Ceram. Soc.* 37, 96 (1954). [5] H. W. Russel, *Journ. of the Am. Ceram. Soc.*, 18, no. 1, 1935 [6] Beck, A.E., 1976, Geophys., *41*, 133. [7] [8] A.D. Brailsford, K.G. Major (1964), *Br. J. Appl. Phys.* 15, 313–319. [9] Sirono, S., and T. Yamamoto, *Plan. Sp. Sc.*, *45* (7), 827-834, 1997. Woodside, W. and Messer, J.H. (1961), *J. Appl. Phys*., 32, 1688. [10], Presley, M.R. and Christensen, P.R. (1997) *J. Geophys. Res.*, 102, E3, 6551-6556.